ACADEMIC PRESS

Available online at www.sciencedirect.com

SCIENCE DIRECT®

Journal of Sound and Vibration 269 (2004) 1063–1081

JOURNAL OF SOUND AND VIBRATION

www.elsevier.com/locate/jsvi

An embedded sensitivity approach for diagnosing system-level vibration problems

C. Yang[a], D.E. Adams[a,*], S.-W. Yoo[a], H.-J. Kim[b]

[a] *Purdue University, School of Mechanical Engineering, Ray W. Herrick Laboratories, 180 S. Intramural Dr., West Lafayette, IN 47907-2031, USA*

[b] *ArvinMeritor, Systems Engineering, 950 W 450 S, Columbus, IN 47401, USA*

Received 15 July 2002; accepted 24 January 2003

Abstract

In diagnosing a system-level vibration problem, the goals are to identify which component or components(s) are most responsible for the phenomenon and which changes to the system are most likely to mitigate the problem. The use of sensitivity analysis in diagnosing system-level vibration phenomena is examined in this work. It is shown that even if only a small subset of measured system input–output functions is available, an appropriate analytical parameterization of these functions leads to simple relationships between the measured data and the desired embedded sensitivity functions. These functions are then reformulated in terms of transmissibility functions with respect to a single input using a novel modal deflection chain technique in order to accommodate system-level operating response data in the absence of input measurements. The embedded sensitivity approach is used to examine two competing design modifications for reducing a structure-borne noise problem in an exhaust system. The sensitivity analysis shows that although both modifications mitigate the resonant vibration problem of interest, one of the modifications is more effective than the other because it introduces less overall change in the forced response characteristics at other frequencies.

1. Introduction

1.1. General

System-level vibration occurs whenever two or more components are assembled into a dynamic system, which is then made to oscillate freely with initial conditions or through forcing of some

*Corresponding author. Tel.: +765-496-6033; fax: +765-494-0787.

E-mail addresses: yang21@purdue.edu (C. Yang), deadams@ecn.purdue.edu (D.E. Adams), sung-woo.yoo@arvinmeritor.com (S.-W. Yoo), han-jun.kim@arvinmeritor.com (H.-J. Kim).

0022-460X/03/$ - see front matter
doi:10.1016/S0022-460X(03)00220-7

kind. In bottom-up industries like the automotive industry, in which many components are designed to avoid system-level resonances at operating excitation frequencies of the engine/powertrain and road spectra using modal charts, vibration problems still occur when changes to one or more components are made late in the design cycle or in new models of previous vehicles by one or more suppliers. These vibration problems can occur anywhere within the system, not just in the modified components, because any change influences the way all of the components interact. The noise, vibration, and harshness (NVH) analysis, testing, and design challenges are to diagnose the problem with limited data and then identify sets of design modifications that are effective at suppressing the problem of interest, but modest enough to avoid new problems without making costly prototypes to validate the proposed changes. Moreover, the goal of this work is to diagnose vibration problems by identifying the parameters to which vibration phenomena are most sensitive, given only system-level (i.e., input–output or output-only) measurements and a parameterization of the subsystems in the absence of full system analytical or numerical (finite element) models.

As an example of a specific scenario in the automotive industry of the general type just described, consider a change in the static stiffness of the suspension in a standard vehicle model that is made to produce a sportier new model with stiffer handling. This change in the suspension subsystem can shift many of the vehicle resonant frequencies of the standard model to undesirable locations. In this scenario, modifications to other components like the exhaust system and engine/powertrain mounting must be made in addition to those in the suspension spring rate to avoid system-level vibration problems. Because an infinite number of design modifications could be made to the components excluding the suspension, it is challenging for suppliers to decide which change should be made to their component to most effectively address the problem without access to models of all subsystems involved. In the absence of shared full system models amongst the suppliers and the vehicle manufacturers, prototypes are usually fabricated and tested in a costly and time-consuming iterative redesign process.

The work here experimentally estimates the sensitivity of a given vibration phenomenon to a component design parameter (mass, damping, stiffness) throughout a frequency range of interest. FRFs in the full system are first measured and then manipulated to provide the desired sensitivity functions to perturbations in design parameters over which suppliers generally have some control. This empirical sensitivity technique is less expensive and faster to implement than the iterative approach and can work backwards from system-level measurements (hence the term 'embedded'), *even when input measurements are unavailable* if operating data is used, to help identify the most promising design modifications given limited amounts of input–output data from the system.

1.2. Description of approach

Impedance modelling, sub-structuring, component-mode synthesis and other analytical and empirical methods are all examples of so-called 'bottom-up' techniques for combining subsystem models to obtain full system models. Force (compatibility) and motion (continuity) constraints are analytically enforced at the connection degrees-of-freedom (d.o.f.s) in order to implement these techniques. The technique developed here is the reverse of these techniques in the sense that system-level measurements are used to quantify the effects of subsystem changes on overall system vibration characteristics in a 'top-down' procedure. In the class of bottom-up methods,

measurements of *subsystem* FRFs (e.g., chassis, exhaust, powertrain) are required whereas in the top-down method discussed here, measurements of *full system* FRFs or operating responses are needed. Note, however, that the embedded sensitivity approach is developed using math-based perturbation, or sensitivity, analysis rather than physics-based force/motion constraints at the connection d.o.f.s, which often have complicated physics of their own as in the case of engine mounts, for example.

The work here gives an alternative, more heuristic derivation of the embedded mass, damping and stiffness sensitivity functions than the one already found in the literature beginning with a linear single degree-of-freedom (s.d.o.f.) vibrating system. The general formula for embedded sensitivities in multiple degree-of-freedom (m.d.o.f.) systems is then given and adapted using transmissibility functions with modal deflection chain conversions for experimental cases, in which only response data are available. Lastly, a case study involving an exhaust subsystem is discussed and a five-d.o.f. model is used to demonstrate the transmissibility-based implementation of the technique. Embedded sensitivity functions for the exhaust subsystem are then calculated and discussed to demonstrate the advantages of one proposed design modification over another to remedy a given vibration resonance problem.

1.3. Literature review

Various theoretical and experimental sensitivity analysis techniques for mechanical vibrations have been discussed in the literature. The concept of receptance sensitivity and a method for its calculation was discussed by Yoshimura for the case of harmonic excitation [1]. Receptance sensitivity was further investigated in its application to structural finite element model updating by Lin and Ewins [2]. In substructuring approaches, which are also referred to as component receptance sensitivity methods, Chang and Park [3] separated a system into two kinds of substructures, modification components and non-modification components. The receptance sensitivity of the whole structure, with respect to the input parameters, was expressed as the product of the receptance sensitivity of the unmodified structure with respect to the interface d.o.f.s and that of the interface d.o.f.s with respect to the input parameters on the modified components.

One method for component mode synthesis was developed by Mace and Shorter [4]. In this work, the FRFs of each subsystem were expressed in terms of the subsystem modes and the system modes were expressed in terms of the subsystem modes using component mode synthesis. A perturbation relationship was then derived to relate small changes in the subsystem modal properties to changes in the global modal properties.

Many research efforts have also focused on the development and application of eigenvalue and eigenvector sensitivity analysis. For example, Jahn [5] derived complete formulae for first order eigenvalue and eigenvector sensitivities for standard eigenvalue problems and then applied them to improve an approximate set of eigenvalues and eigenvectors. The theory was later extended by Fox and Kapoor [6] to the case of generalized symmetric eigenvalue problems by considering changes of physical parameters in the mass and the stiffness matrices.

Though these existing methods have proven to be very useful, they are restricted to cases where accurate analytical or finite element models are available. In many practical applications where sensitivities are needed to remedy noise and vibration problems, only limited *experimental* data

are available. A general method for using limited amounts of data was developed by Lin and Lim [7] to estimate both FRF sensitivities and eigenvalue/eigenvector sensitivities from vibration test data. Their work was based on earlier observations by Vanhonaker [8], Belle and Liu [9], and Lim and Liew [10]. Design sensitivities were calculated directly from measured data and the relationship between the FRF sensitivities and eigenvalue and eigenvector sensitivities was established. A modal acceleration method for the frequency responses and a double-modal acceleration method for their sensitivities in undamped systems were also derived by Qu [11]. Similar methods for viscously damped systems were derived by Qu and Selvam [12]. The two methods were based on a hybrid expansion, which involved a power series expansion and modal superposition, of the flexibility matrix.

The work here contributes to the literature by first providing an alternative more heuristic, physics-based derivation of embedded sensitivity functions to that in Ref. [7]; second, reformulating the sensitivity functions in terms of transmissibility functions to accommodate the use of operating data in which input measurements are not usually available; third, discussing a practical experimental application of the sensitivity functions for diagnosing a vibration problem in an exhaust system; and then fourth, implementing the transmissibility-based sensitivity technique using operating data only. The authors have also extended the use of embedded sensitivity functions to non-linear systems [13]; however, this work is being presented elsewhere.

2. Embedded sensitivity theory

Embedded sensitivity functions are derived here in terms of FRFs because these are commonly measured and computed analytically to diagnose noise and vibration problems in many applications. These sensitivity functions indicate the variation in FRF magnitude and phase with respect to perturbations in mass, damping, and stiffness parameters. The term 'embedded' is used here to refer to the sensitivity functions because they are explicit functions of the FRFs; thus the individual mass, damping, and stiffness parameters are not needed to compute the sensitivity functions in contrast to the requirement for a full analytical or numerical model in typical parametric design studies.

2.1. S.d.o.f. derivation

To illustrate the derivation of embedded sensitivity functions in terms of FRFs, first consider the linear time-invariant s.d.o.f. system model in the absence of gyroscopic forces shown in Fig. 1(a). Although this system is assumed to have equivalent viscous damping, other forms of linear damping also fit within the framework of this approach. Refer to Ref. [8] for a general derivation of these sensitivity functions in terms of impedance functions. The linear, second order, ordinary differential equation of motion associated with this model is given by

$$M_1\ddot{y}_1 + C_1\dot{y}_1 + K_1 y_1 = f_1(t), \tag{1}$$

where M_1, C_1, and K_1 are the mass, equivalent viscous damping, and stiffness parameters; f_1 is the force excitation; and y_1 is the displacement response. The desired embedded sensitivity functions

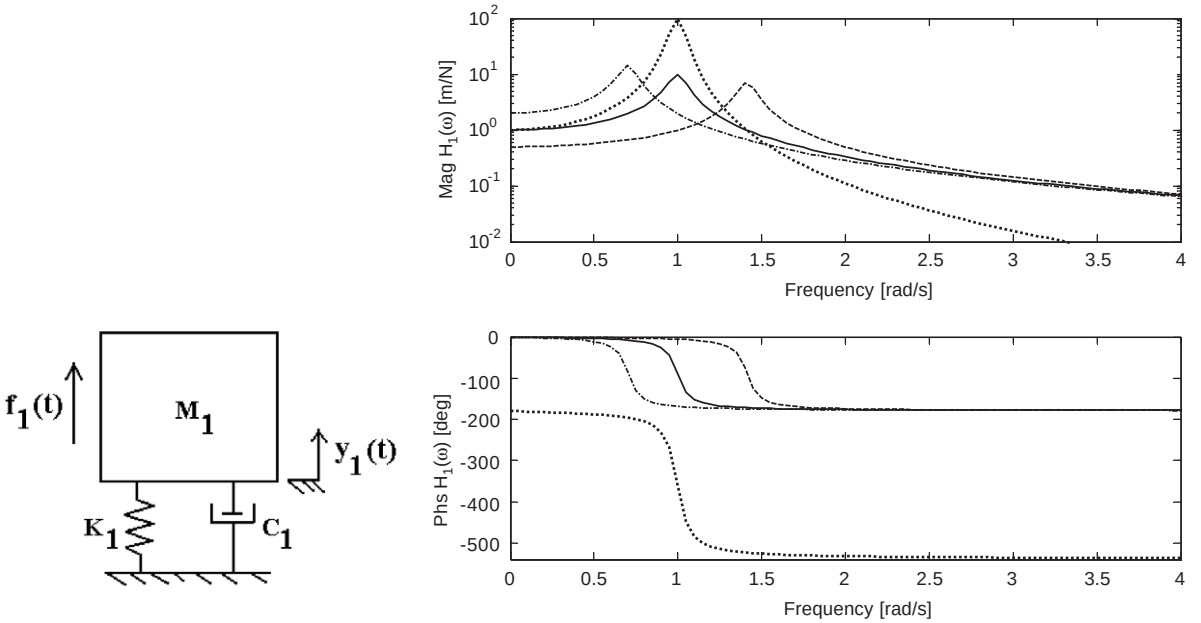

Fig. 1. (a) Schematic of an s.d.o.f. linear system model; (b) magnitude and phase plots of an s.d.o.f. FRF for $K_1 =$ 1 N/m (_), $K_1 = 2$ N/m (- - -), and $K_1 = 0.5$ N/m (-.-) with the corresponding embedded sensitivity function, $\partial H_1/\partial K_1$ (…), for the system stiffness parameter.

that will be derived below should describe how the input–output relationship between f_1 and y_1 varies in both magnitude and phase as M_1, C_1 or K_1 varies.

The corresponding FRF between f_1 and y_1, which is found by taking the ratio of the Fourier transform of the harmonic response to that of the excitation, is given by the familiar formula

$$\frac{Y_1(\omega)}{F_1(\omega)} = H_1(\omega) = \frac{1}{K_1 - \omega^2 M_1 + \mathrm{j}\omega C_1}. \tag{2}$$

The first parameter for which a sensitivity function will be found is the stiffness, K_1. In order to provide some insight into the nature of this stiffness sensitivity function, plots of the magnitude and phase of $H_1(\omega)$ as functions of frequency are shown in Fig. 1(b) for three different values of K_1, 1 N/m (_), 2 N/m (- - -), and 0.50 N/m (-.-), with fixed $M_1 = 1$ kg and $C_1 = 0.1$ N s/m. These plots simply show that increases in K_1 cause the undamped natural frequency, $\omega_n = \sqrt{K_1/M_1}$, to increase and also cause the low-frequency static stiffness line in the magnitude plot to decrease according to $1/K_1$. These three plots also show that stiffness has little effect on the frequency response for high frequencies where inertia forces dominate.

The sensitivity function of the FRF in Eq. (2) to variations in stiffness, ΔK_1, is found by taking the partial derivative of $H_1(\omega)$ with respect to K_1:

$$\frac{\partial H_1(\omega)}{\partial K_1} = \frac{-1}{(K_1 - \omega^2 M_1 + \mathrm{j}\omega C_1)^2} = -H_1^2(\omega). \tag{3}$$

Note that the resulting sensitivity function can be expressed explicitly in terms of the FRF, $H_1(\omega)$, and does not require knowledge of any of the system parameters within the model. The only requirement in taking the partial derivatives was that the parametric form of the FRF in terms of the parameters be known. Furthermore, this type of parameterization is often known in practical applications of the type envisioned by this research.

Plots of the magnitude and phase of $\partial H_1/\partial K_1$ as functions of frequency (…) are shown in Fig. 1, overlaid with the FRFs for three different values of the stiffness parameter. Note that the sensitivity function clearly indicates that variations in stiffness do not significantly affect the high-frequency portion of the FRF in magnitude or in phase. The high sensitivity near the peak of the FRF is also reflected in the plot, as is the uniform decrease in the low-frequency portion of the FRF magnitude. The mass and damping sensitivity functions are provided below in Eqs. (4a) and (4b) and can be interpreted in the same way as the stiffness sensitivity function:

$$\frac{\partial H_1(\omega)}{\partial C_1} = \frac{-\mathrm{j}\omega}{(K_1 - \omega^2 M_1 + \mathrm{j}\omega C_1)^2} = -\mathrm{j}\omega H_1^2(\omega),$$
$$\frac{\partial H_1(\omega)}{\partial M_1} = \frac{-\omega^2}{(K_1 - \omega^2 M_1 + \mathrm{j}\omega C_1)^2} = \omega^2 H_1^2(\omega). \quad (4a, b)$$

2.2. Two-d.o.f. system derivation

The s.d.o.f. example in Section 2.1 was interesting but does not have much practical value for diagnosing system-level noise and vibration problems because these problems always involve more than one d.o.f. Fortunately, the technique used above to derive the embedded sensitivity functions for variations in mass, damping and stiffness in the s.d.o.f. case generalizes to higher order systems like the two-d.o.f. system model shown in Fig. 2(a). The equations of motion of this system are given in matrix form by

$$\begin{bmatrix} M_1 & 0 \\ 0 & M_2 \end{bmatrix} \begin{Bmatrix} \ddot{y}_1 \\ \ddot{y}_2 \end{Bmatrix} + \begin{bmatrix} C_1 + C_2 & -C_2 \\ -C_2 & C_2 \end{bmatrix} \begin{Bmatrix} \dot{y}_1 \\ \dot{y}_2 \end{Bmatrix} + \begin{bmatrix} K_1 + K_2 & -K_2 \\ -K_2 & K_2 \end{bmatrix} \begin{Bmatrix} y_1 \\ y_2 \end{Bmatrix} = \begin{Bmatrix} f_1(t) \\ f_2(t) \end{Bmatrix}, \quad (5)$$

where the mass, equivalent viscous damping, and stiffness parameters and response and excitation variables correspond to those shown schematically in Fig. 2. The FRF input–output equation that relates harmonic excitations at $f_1(t)$ and $f_2(t)$ to harmonic responses, $y_1(t)$ and $y_2(t)$ in the steady state, consistent with this set of linear ordinary differential equations is given by

$$\begin{Bmatrix} Y_1(\omega) \\ Y_2(\omega) \end{Bmatrix} = \frac{1}{\Delta(\omega)} \begin{bmatrix} K_2 - \omega^2 M_2 + \mathrm{j}\omega C_2 & \mathrm{j}\omega C_2 + K_2 \\ \mathrm{j}\omega C_2 + K_2 & K_1 + K_2 - \omega^2 M_1 + \mathrm{j}\omega(C_1 + C_2) \end{bmatrix} \begin{Bmatrix} F_1(\omega) \\ F_2(\omega) \end{Bmatrix}$$
$$= \begin{bmatrix} H_{11}(\omega) & H_{12}(\omega) \\ H_{21}(\omega) & H_{22}(\omega) \end{bmatrix} \begin{Bmatrix} F_1(\omega) \\ F_2(\omega) \end{Bmatrix}, \quad (6)$$

where $\Delta(\omega) = (K_1 + K_2 - \omega^2 M_1 + \mathrm{j}\omega(C_1 + C_2)).\ (K_2 - \omega^2 M_2 + \mathrm{j}\omega C_2) - (\mathrm{j}\omega C_2 + K_2)^2$ is the characteristic polynomial in terms of the circular frequency (rad/s), ω. This characteristic polynomial can be set equal to zero to compute the modal frequencies.

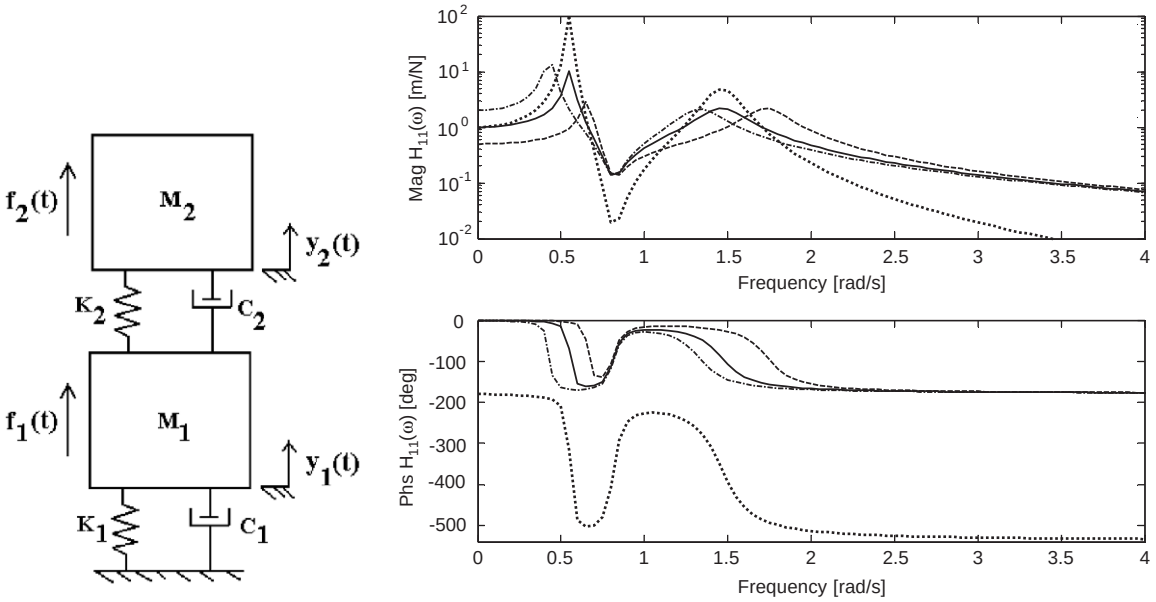

Fig. 2. (a) Schematic of a two-d.o.f. linear system model; (b) magnitude and phase plots of two-d.o.f. FRF: $H_{11}(\omega)$, for $K_1 = 1\,\mathrm{N/m}$ (_), $K_1 = 2\,\mathrm{N/m}$ (- - -), and $K_1 = 0.5\,\mathrm{N/m}$ (-.-) with the corresponding embedded sensitivity function, $\partial H_{11}/\partial K_1$ (…), for the system stiffness parameter, K_1.

The embedded stiffness sensitivity functions of the three unique FRFs for this system, $H_{11}(\omega)$, $H_{12}(\omega)$, and $H_{22}(\omega)$, to variations in K_1 are derived below in Eqs. (7)–(9):

$$\frac{\partial H_{11}(\omega)}{\partial K_1} = \frac{-(K_2 - \omega^2 M_2 + \mathrm{j}\omega C_2)^2}{\Delta^2(\omega)} = -H_{11}^2(\omega), \tag{7}$$

$$\frac{\partial H_{12}(\omega)}{\partial K_1} = \frac{-(\mathrm{j}\omega C_2 + K_2)(K_2 - \omega^2 M_2 + \mathrm{j}\omega C_2)}{\Delta^2(\omega)} = -H_{11}(\omega)H_{12}(\omega), \tag{8}$$

$$\frac{\partial H_{22}(\omega)}{\partial K_1} = \frac{\Delta(\omega) - (K_1 + K_2 - \omega^2 M_1 + \mathrm{j}\omega(C_1 + C_2))(K_2 - \omega^2 M_2 + \mathrm{j}\omega C_2)}{\Delta^2(\omega)}$$
$$= \frac{-(\mathrm{j}\omega C_2 + K_2)^2}{\Delta^2(\omega)} = -H_{12}^2(\omega). \tag{9}$$

Before proceeding to plot the stiffness sensitivity function results for the two-d.o.f. linear system model, the form of the functions in Eqs. (7)–(9) should first be noted. All of these embedded functions are by definition explicit functions of the original set of FRFs, $H_{11}(\omega)$, $H_{12}(\omega)$, and $H_{22}(\omega)$; thus, the sensitivities of these FRFs to variations in K_1 can be calculated directly from the FRFs without the need for specific parameter values.

Fig. 2(b) shows the magnitudes and phases of the system FRF, $H_{11}(\omega)$, for different values of K_1, 1, 2, and 0.50 N/m, with fixed $M_1 = 1\,\mathrm{kg}$, $M_2 = 1.2\,\mathrm{kg}$, $C_1 = 0.1\,\mathrm{N\,s/m}$, $C_2 = 0.1\,\mathrm{N\,s/m}$, and $K_2 = 0.8\,\mathrm{N/m}$ in addition to the embedded stiffness sensitivity, $\partial H_{11}(\omega)/\partial K_1$. The sensitivity function is seen to exhibit similar characteristics as in the s.d.o.f. example in Fig. 1. For instance,

consider how the magnitude and phase plots for $\partial H_{11}(\omega)/\partial K_1$ in Fig. 2 determine the sensitivity of $H_{11}(\omega)$ to variations in K_1. Note that near the first peak of $||H_{11}(\omega)||$, where $||H_{11}(\omega)||$ denotes the magnitude of $H_{11}(\omega)$, at 0.55 rad/s for $K_1 = 1$ N s/m, the sensitivity in magnitude to changes in K_1 is relatively large, a fact that is verified by the three plots of $||H_{11}(\omega)||$ for different stiffness values. In contrast, the sensitivity in magnitude to changes in K_1 is relatively small near the second peak of $||H_{11}(\omega)||$ at 1.45 rad/s. Furthermore, the magnitude of the sensitivity function at the antiresonance (complex-zero), which is created by the $(K_2 - \omega^2 M_2 + j\omega C_2)$ polynomial in the numerator of $\partial H_{11}(\omega)/\partial K_1$ in Eq. (8), is small; so there is practically no change in $||H_{11}(\omega)||$ near 0.8 rad/s.

2.3. Derivation for third and higher d.o.f. systems

The s.d.o.f. and two-d.o.f. systems discussed in Sections 2.1 and 2.2 both generated embedded sensitivity functions that described how changes in system parameters caused the system FRFs to change given only the system input–output/FRF measurements. The sensitivity functions become more complicated for three or more d.o.f.s but the derivation is similar.

Consider the linear three-d.o.f. system model shown in Fig. 3, noting that the parameter labels have been modified relative to those in Figs. 1 and 2 to more explicitly indicate coupling within the system. In general, K_{jk} is the stiffness between d.o.f.s k and j, and the viscous damping coefficients are similarly defined. An index of '0' is used in the stiffness and damping parameters associated with the boundary condition, K_{10} and C_{10}, because the coupling in these cases is between ground and d.o.f. 1. Also note that the mass parameters, M_{j0}, are all expressed with respect to ground because the inertial terms are defined with respect to the inertial reference frame.

The sensitivity functions for $H_{jk}(\omega)$ can be found by extending the results for the single and two-d.o.f. systems. By carrying out the various sensitivity derivations, it can be shown that the general sensitivity functions of $H_{jk}(\omega)$ with respect to the coupling parameter, P_{mn} (e.g., M_{m0}, C_{mn}, K_{mn}), are computed using the equations

$$\frac{\partial H_{jk}}{\partial K_{mn}} = -[H_{jm}(\omega) - H_{jn}(\omega)][H_{km}(\omega) - H_{kn}(\omega)] \quad \text{with } H_{j0}(\omega) \equiv 0,$$
$$\frac{\partial H_{jk}}{\partial C_{mn}} = j\omega \frac{\partial H_{jk}}{\partial K_{mn}},$$
$$\frac{\partial H_{jk}}{\partial M_{m0}} = (j\omega)^2 \frac{\partial H_{jk}}{\partial K_{m0}}. \tag{10a–c}$$

Ref. [7] gives these expressions in a different form in terms of the system FRF matrix.

2.4. Reformulation for use with operating data

The expressions in Eqs. (10a-c) relate the embedded sensitivity functions to input–output FRF measurements, which can often be easily measured in the laboratory for subsystems such as the exhaust system discussed in Section 3. FRFs are, however, difficult to measure in systems with internal inputs as in the case of rotational imbalance forces in powertrain chassis dynamometer testing or inputs at the tire patch during road testing. Moreover, operating data are often acquired in many tests conducted by the automotive and supplier industries, because these data more

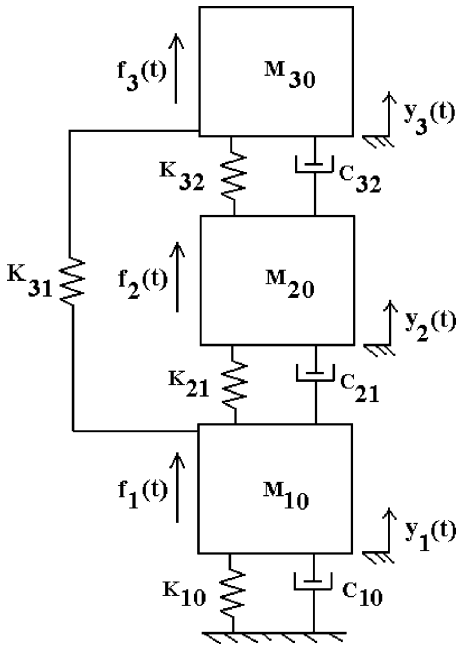

Fig. 3. Schematic of a three-d.o.f. linear system model with an alternative parameter labeling format used to emphasize coupling.

accurately reflect the true dynamic loads and levels to which vehicle systems or subsystems are exposed. The embedded sensitivity functions in Section 2.3 are reformulated using modal deflection chains in this section to make use of operating data rather than FRF data.

First, the sensitivity formula in Eq. (10a) can be rewritten in terms of the respective transmissibility functions and operating responses as follows:

$$\begin{aligned}\frac{\partial H_{jk}}{\partial K_{mn}} &= -[H_{jm}(\omega) - H_{jn}(\omega)][H_{km}(\omega) - H_{kn}(\omega)] \\ &= -[T_{mj,j}(\omega) - T_{nj,j}(\omega)][T_{mk,k}(\omega) - T_{nk,k}(\omega)]H_{jj}(\omega)H_{qq}(\omega) \\ &= -\frac{[X_{mj}(\omega) - X_{nj}(\omega)][X_{mk}(\omega) - X_{nk}(\omega)]}{F_j(\omega)F_k(\omega)},\end{aligned} \tag{11}$$

where

$$\begin{aligned}&T_{mk,k}(\omega) = \frac{X_m(\omega)}{X_k(\omega)} = \frac{H_{mk}(\omega)F_k(\omega)}{H_{kk}(\omega)F_k(\omega)} = \frac{H_{mk}(\omega)}{H_{kk}(\omega)} \text{ for input at d.o.f. } k, \\ &T_{jj,q}(\omega) = 1 = T_{kk,q}(\omega) \text{ for all } q \quad \text{and} \quad T_{mk,k}(\omega) = 1/T_{km,k}(\omega).\end{aligned} \tag{12}$$

The formulae in Eq. (11) are useful if data are available for two different input d.o.f.s, j and k. Note that only the numerator in the last line of Eq. (11) is needed when determining the relative sensitivity of the system to changes in stiffness parameters, K_{mn}, because the denominator is common to all of these parameter sensitivities. Although this equation is useful for laboratory subsystem testing, it is difficult to obtain this type of data in large systems with many components because inputs at certain d.o.f.s can sometimes not be applied at all or when they are applied do

not adequately excite all of the components (i.e., inputs are not persistent). In order to overcome this difficulty, the sensitivity functions in Eq. (11) can be converted into expressions involving only a single input reference using a transformation based on the modal deflection shapes of the system.

To that end, note that near each mode of vibration of the system, the following equalities hold depending on the amplitude of the j and k inputs because no matter which input is applied to the system, the individual mode shapes are identical whereas the scaling of those modes is different:

$$\frac{X_{mk}(\omega) - X_{nk}(\omega)}{\|X_{kk}(\omega)\|} = \frac{X_{mj}(\omega) - X_{nj}(\omega)}{\|X_{kj}(\omega)\|}.$$
$$\frac{X_{mk}(\omega) - X_{nk}(\omega)}{\|X_{jk}(\omega)\|} = \frac{X_{mj}(\omega) - X_{nj}(\omega)}{\|X_{jj}(\omega)\|}. \quad (13a, b)$$

These relationships are referred to in this paper as modal deflection chains because they provide a means to transform the embedded sensitivity functions into expressions that are more useful in practical engineering NVH tests. For example, if Eq. (13a) is substituted into Eq. (11), the following result is obtained:

$$\frac{\partial H_{jk}}{\partial K_{mn}} = -[T_{mk,k}(\omega) - T_{nk,k}(\omega)]^2 \|H_{kk}(\omega)H_{jk}(\omega)\|. \quad (14)$$

Thus, the only data needed to compare the effects of various changes in the system stiffness parameters, K_{mn}, are the transmissibility measurements between the mth and kth and nth and kth d.o.f.s due to an input at d.o.f. k. The common factor, $H_{kk}(\omega)H_{jk}(\omega)$, need not be considered in a relative sensitivity study. For this reason, Eq. (14) is a very useful expression in spite of its simplicity, as is illustrated below in Section 3.2.

3. Application of embedded sensitivity analysis

An exhaust subsystem is experimentally analyzed in this section using embedded sensitivity functions. Then a five-d.o.f. simulation example system is analyzed using transmissibility-based relative embedded sensitivity functions from Eq. (14). The exhaust subsystem under investigation is shown in Fig. 4(a). Note that the exhaust has been supported with elastic cords to approximate free–free boundary conditions by isolating the exhaust from the test frame.

Before proceeding to analyze forced response data from the exhaust system, it is worthwhile to consider the nature of the noise and vibration problem of interest. The first generation design of this exhaust subsystem, which was installed in a standard compact vehicle model, did not exhibit a resonance problem in the 300–350 Hz range. When the suspension of the standard vehicle system was modified to produce a sportier model, a vibration problem in the rear floorboard of the newer model appeared with an accompanying structure-borne noise problem inside the saloon. Because the noise problem was created by a necessary change to the suspension system, a modification to the exhaust subsystem was required to mitigate the problem. After several design modifications were made to the exhaust, a successful design, which involved a flexible Metex joint at the inlet pipe to the muffler, for removing the vibration problem, was identified. The discussion below is a

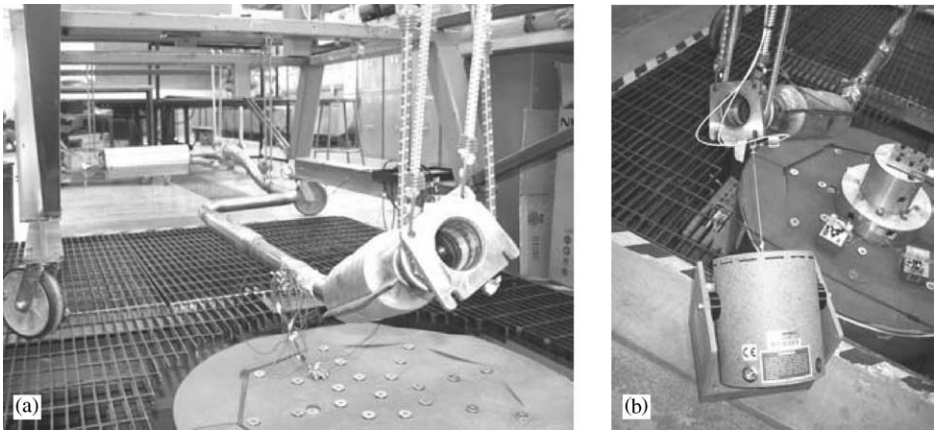

Fig. 4. (a) Photograph of the exhaust subsystem under investigation supported with elastic cords to approximate free–free boundary conditions; (b) electrodynamic shaker attached with stinger to the front bracket of the exhaust system in front of the bellows to simulate input from powertrain.

follow-up analysis of that noise and vibration design scenario using embedded sensitivity functions.

3.1. Exhaust subsystem characteristics

The exhaust subsystem modal characteristics in the frequency range of interest were estimated using FRF measurements in the three Cartesian co-ordinate directions at ten locations (see Fig. 5) not including the skewed driving point input location near the forward bracket of the exhaust (see Fig. 4(b)). A 50 lbf electrodynamic shaker, which was instrumented with a PCB 288D01 impedance head (sensitivity 102.24 mV/lbf, 98.36 mV/g) for measuring force and acceleration at the attachment location, was used to excite the exhaust into vibration to simulate the input from the powertrain, and triaxial accelerometers (PCB model 356A08, sensitivity 92–102 mV/g, PCB model A356B18, sensitivity 907–1042 mV/g) were used to measure three axes of acceleration at each point in Fig. 5. FRFs were computed using a Hanning window with 50% overlap signal processing, 4096 block size, 2048 Hz sampling frequency, and a digital filter with a 800 Hz bandwidth for a 0.5 Hz frequency resolution.

FRFs in the x (longitudinal), y (vertical), and z (lateral) Cartesian co-ordinate directions were estimated for each input–output pair. The magnitude and phase of the $H_{71}(\omega)$, $H_{81}(\omega)$, $H_{91}(\omega)$, and $H_{101}(\omega)$ FRFs in the y direction are plotted in Fig. 6. Note the peak in all of the FRFs near 312 Hz. The relative deflection mode shape associated with this particular damped modal frequency is shown in Fig. 7 in all the three directions. These shapes were obtained using the peak-pick modal parameter estimation method [13] in which the imaginary parts of the associated FRFs, $imag\, H_{n,1}(\omega)$, are taken to be the modal deflection coefficients at resonant peaks; this s.d.o.f. approach was valid near 312 Hz because that mode is dominant at that frequency. The first interesting characteristic to note about this mode shape is that it has contributions from all the three co-ordinate directions. Second, note that the x direction (longitudinal) mode shape has a rather large deflection at the input location compared to the other locations, indicating that the

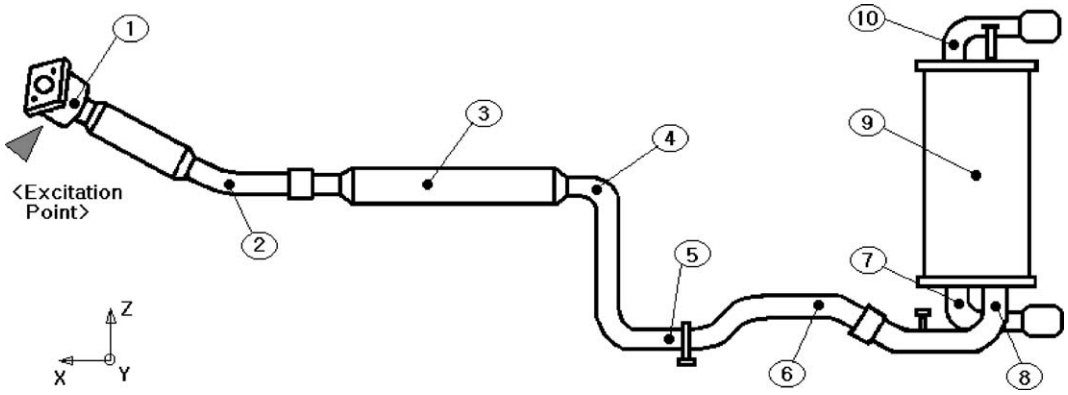

Fig. 5. Illustration of measurement d.o.f. used in tests on an exhaust subsystem; tri-axial acceleration measurements were made at each point.

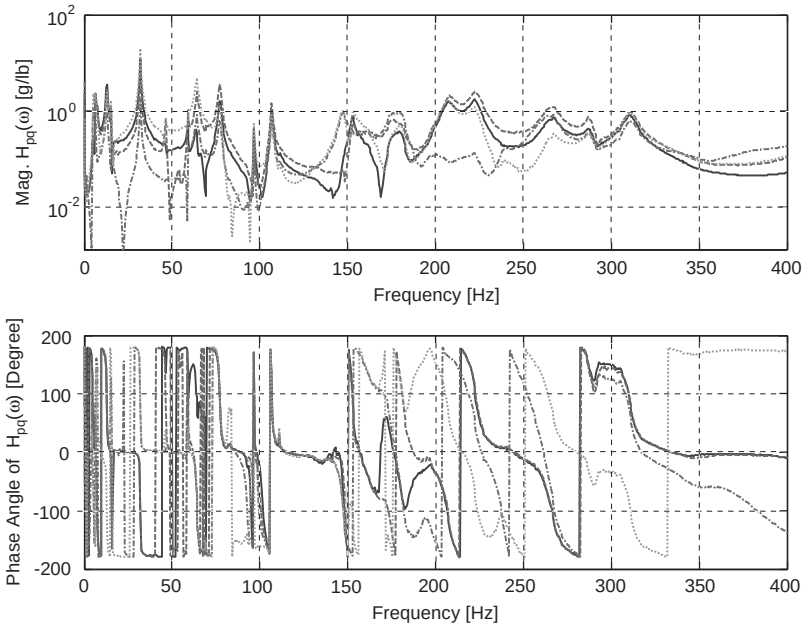

Fig. 6. Magnitude and phase of y direction frequency response functions: (_) $H_{71}(\omega)$, (- - -) $H_{81}(\omega)$, (…) $H_{91}(\omega)$, and (-.-) $H_{10,1}(\omega)$ with a skewed input.

bellows, which are compliant in the x direction, isolates the exhaust system in that direction at that frequency. Third, note that the y direction (vertical) mode shape near 312 Hz exhibits a large relative deflection from the inlet pipe to the muffler across to the outlet pipe. This large torsional motion suggests that the inlet to the muffler may be a region to modify in order to shift this modal frequency out of the 300–350 Hz frequency range; however, the mode shape alone does not indicate what the ramifications are at the other frequencies of shifting this mode. In contrast, embedded sensitivity functions do provide this type of information.

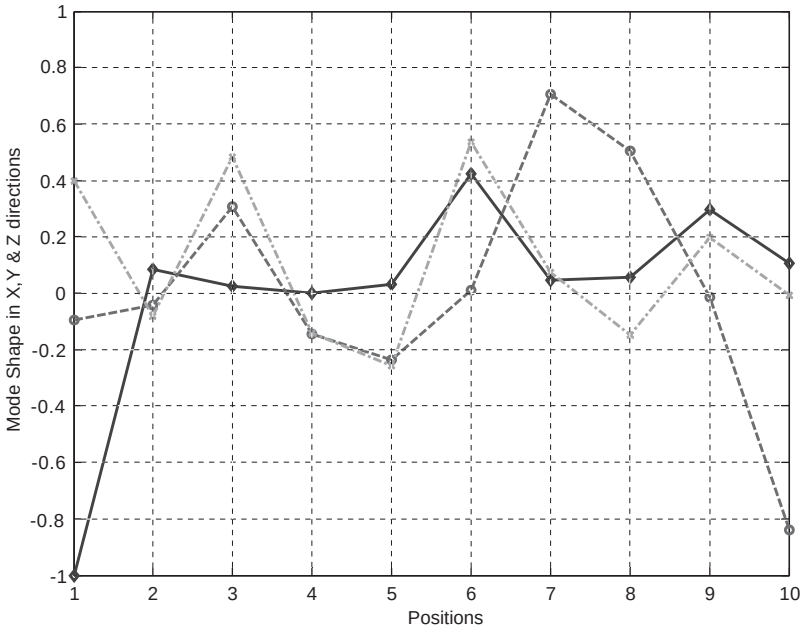

Fig. 7. Relative deflection mode shapes in (_) x, (- - -) y, and (-.-) z directions estimated using the imaginary parts (peak-pick method) of the associated FRFs (normalized).

3.2. Embedded sensitivity analysis with measured FRFS

As was previously mentioned, a relative modal deflection shape in a linear vibrating system gives a clear indication of whether or not a parameter change (mass, stiffness, damping) to the system will affect that mode of vibration. In general, a change in the system at a frequency for which there is large relative motion will produce significant changes at that frequency; however, there are two important pieces of design information that are not obtained using this modal approach: (1) the effects on frequencies/modes other than the problem frequencies/modes; (2) the carry-over effects of lower frequencies on higher frequencies (e.g., static stiffness at the boundary condition). Embedded sensitivity functions provide these other pieces of information because they are computed using all of the frequency response data rather than just the data near certain modes. The baseline and modified exhaust systems are now examined in light of the experimentally obtained embedded sensitivities to define the most effective changes.

In order to propose a design modification to the exhaust system that would affect the 312 Hz mode, several sets of embedded sensitivity functions were computed and examined. Initially, it was thought that a change in the stiffness of the bellows could potentially help to shift this mode out of the 300–350 Hz frequency range. The sensitivity function for stiffness changes towards the front of the exhaust system (path between points 1 and 2 in Fig. 5) was computed using the formula

$$\frac{\partial H_{81}}{\partial K_{12}} = -[H_{81}(\omega) - H_{82}(\omega)][H_{11}(\omega) - H_{12}(\omega)]. \tag{15}$$

Note that the FRFs, $H_{81}(\omega)$, $H_{11}(\omega)$, $H_{12}(\omega)$, $H_{82}(\omega)$, were measured using modal impact testing for convenience as were the other FRFs in the sensitivity functions below.

The sensitivity function of the same FRF, $H_{81}(\omega)$, to changes in the exhaust system at the inlet pipe to the muffler (path between points 8 and 9 in Fig. 5) was also computed using the expression

$$\frac{\partial H_{81}}{\partial K_{89}} = -[H_{88}(\omega) - H_{89}(\omega)][H_{18}(\omega) - H_{19}(\omega)]. \tag{16}$$

Both of the stiffness sensitivity functions from Eqs. (15) and (16) are plotted in Fig. 8 for comparison. Note that although the sensitivity of the FRF to changes in the bellows is relatively high in the 200–250 Hz frequency range, the sensitivity to changes across the bellows near 312 Hz is low. This low sensitivity suggests that changes to the bellows are not the most effective way to deal with the vibration problem. Furthermore, Fig. 8 indicates that changes to the muffler inlet pipe are more effective than changes to the bellows at modifying/shifting the resonance near 312 Hz for two reasons. First, the magnitude of the sensitivity of $H_{81}(\omega)$ to K_{89} is relatively large at 312 Hz, and second, the sensitivity function for changes to the muffler inlet in other frequency ranges is small compared to the corresponding sensitivity function for the change to the bellows. In fact, the change near the muffler has its greatest impact on the vibrations at 312 Hz whereas the change in the bellows makes a significant impact at many other frequencies as well; these broad changes are likely to create new vibration problems at other input frequencies of the powertrain.

These conclusions using embedded sensitivity functions were also confirmed with the experimentally determined FRFs for the exhaust system with a Metex joint inserted at the inlet

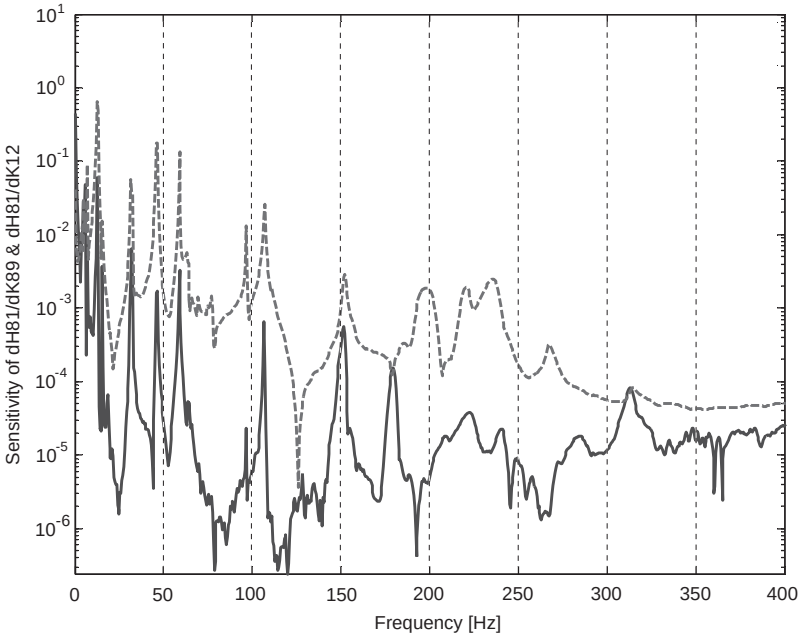

Fig. 8. Comparison of stiffness sensitivity functions of the exhaust system to changes near the bellows (- - -) and the inlet muffler pipe (—).

pipe to the muffler (Fig. 9). Fig. 10 for the modified exhaust should be compared with the baseline FRFs given previously in Fig. 6. Note that the peak in the neighborhood of 312 Hz has been shifted downward in frequency with the addition of the Metex joint. In other words, the vibration problem was effectively addressed by changing K_{89}.

3.3. Embedded sensitivity analysis with transmissibility functions

The FRFs of the five-d.o.f. system shown in Fig. 11 when excited with an input force at d.o.f. 3 (powertrain) were simulated by inverting the system impedance matrix. The system parameters used in the frequency domain simulation are given in Table 1. Note that the coupling stiffness and damping between d.o.f.s 3 and 4 have been removed in this example because original test observations indicated that the hangers in the exhaust system did not influence the vibration problem of interest; therefore, the design objective was to determine which of the three coupling stiffness parameters, K_{12}, K_{23}, and K_{45}, should be modified. In a typical operational experiment, this vehicle system might be subjected to the powertrain rotating imbalance force, $f_3(t)$, as well as road inputs, which will be ignored here. When Eq. (14) is used to compute the modal-deflection-scaled relative embedded sensitivity, $[X_{mk}(\omega) - X_{nk}(\omega)]^2$ with $k = 3$, for the three stiffness elements, K_{12}, K_{23}, and K_{45}, the results in Fig. 12 are obtained.

Note that these relative sensitivity functions indicate which stiffness modification is the most effective at shifting resonances. For example, the plot in Fig. 12 can be split into three distinct frequency ranges: the first from 0 to 7.5 Hz where K_{12} is most influential; the second from 7.5 to 12.5 Hz where K_{23} is most influential; and the third from 12.5 to 30 Hz where K_{45} is most influential. When these relative sensitivity functions are compared with the absolute sensitivity functions shown in Fig. 13 as computed using Eq. (10a), it is seen that the two results are similar. In fact, the sensitivity function ratios, which determine the relative effectiveness of one stiffness change with respect to another, are identical in this example.

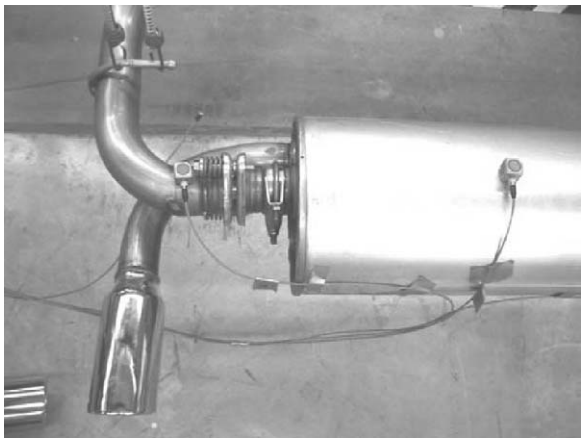

Fig. 9. Photo of inlet pipe of muffler fitted with Metex joint for reducing the exhaust torsional coupling stiffness at that location to mitigate the vibration problem.

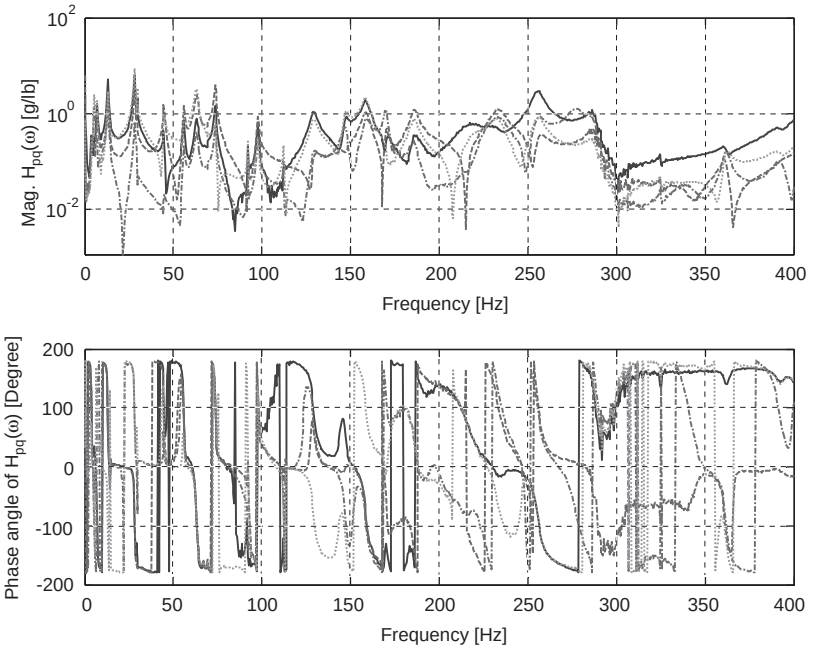

Fig. 10. Magnitude and phase of y direction FRFs: (_) $H_{71}(\omega)$, (---) $H_{81}(\omega)$, (…) $H_{91}(\omega)$, and (-.-) $H_{10,1}(\omega)$ of the modified exhaust system with a Metex joint showing suppression of mode in the 300–350 Hz range.

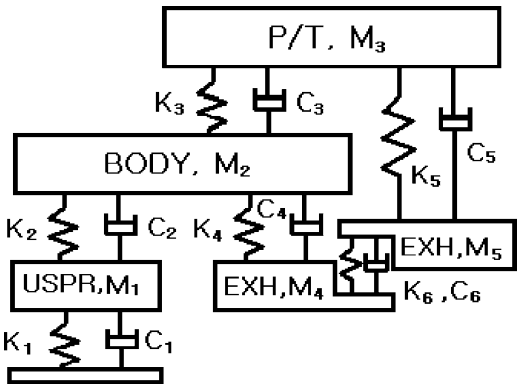

Fig. 11. Simplified five-d.o.f. model of a vehicle system with the exhaust subsystem consisting of two lumped masses.

Table 1
System parameters in simplified five-degree-of-freedom vehicle model

System parameters
$M_1 = 35$, $M_2 = 100$, $M_3 = 110$, $M_4 = 25$, and $M_5 = 30$ kg
$C_1 = 85$, $C_2 = 75$, $C_3 = 105$, $C_4 = 0$, $C_5 = 135$, and $C_6 = 125$ N s/m
$K_1 = 170e3$, $K_2 = 150e3$, $K_3 = 210e3$, $K_4 = 0$, $K_5 = 270e3$, and $K_6 = 250e3$ N/m

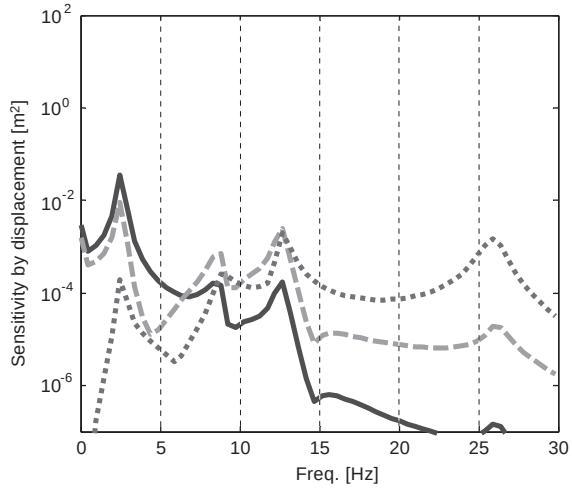

Fig. 12. Relative sensitivity functions from Eq. (14) with modal deflection chain scaling for changes in three coupling stiffness parameters using only displacement spectra from the five-d.o.f. system in Fig. 11 with (_) K_{12}, (- - -) K_{23} and (…) K_{45}.

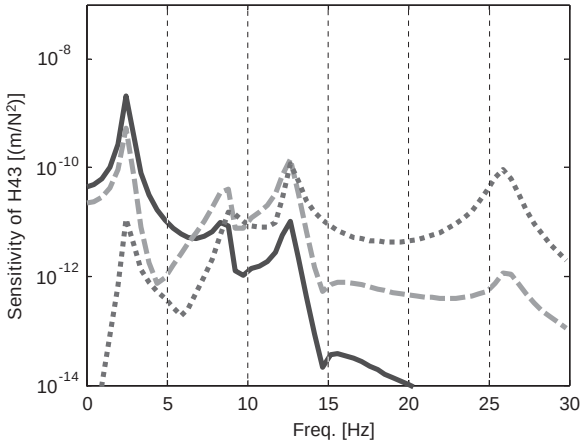

Fig. 13. Absolute sensitivity functions from (10) for changes in three coupling stiffness parameters using only displacement spectra from the five-d.o.f. system in Fig. 11 with (_) K_{12}, (- - -) K_{23} and (…) K_{45}.

Some inconsistencies between the absolute and relative sensitivities have been observed primarily near anti-resonances and in other frequency ranges for which the modes are coupled when the d.o.f.s have both serial and parallel coupling because Eq. (14) was obtained using a modal deflection chain, which is only valid when a single mode is active; therefore, the relative sensitivity functions will be most accurate near resonances and less accurate near anti-resonances. Because noise and vibration problems are usually associated with resonant behavior, these discrepancies in the transmissibility-based sensitivity functions can be ignored in most applications.

4. Conclusions

The use of sensitivity analysis in diagnosing system-level vibration phenomena was examined in this work. A series of vibrating system models were used to derive embedded sensitivity functions for one, two, and larger degree-of-freedom systems. It was shown that the resulting sensitivity functions were 'embedded' because they do not require explicit knowledge of the mass, damping, or stiffness properties of a system, only the frequency response functions. The embedded sensitivity functions were then reformulated in terms of transmissibility functions for multiple inputs and then a single input using modal deflection chains. Embedded sensitivity functions were then used to experimentally compare two different design modifications to the bellows and the muffler inlet of an exhaust subsystem. It was shown that these sensitivity functions indicated which design modification was most effective at shifting a specific modal frequency and also how that modification affected the frequency response behavior at frequencies across the entire frequency range of interest. A five-degree-of-freedom vehicle system model was also used to demonstrate how the transmissibility-based sensitivity formula could be used in the absence of an input measurement. The effects of non-linearity on embedded sensitivity models are being addressed elsewhere by the authors.

Acknowledgements

The authors gratefully acknowledge John Grace, Vice President of Engineering and Technology with ArvinMeritor and Anthony Hicks, Director of Systems Engineering, for supporting this research. This work is dedicated to the memory of Mr. David Strickland (1956–2002), who served for 23 years in Product Engineering, DaimlerChrysler Business Group at ArvinMeritor Technical Center in Columbus, IN.

References

[1] Y. Yoshimura, Design sensitivity analysis of frequency response in machine structures, Journal of Mechanisms, Transmissions and Automation in Design 106 (1984) 119–125.
[2] R.M. Lin, D.J. Ewins, Analytical model improvement using frequency response functions, Mechanical Systems and Signal Processing 8 (1994) 437–458.
[3] K.-J. Chang, Y.-P. Park, Structural dynamic modification using component receptance, Mechanical Systems and Signal Processing V12 (1998) 525–541.
[4] B.R. Mace, P.J. Shorter, A local modal/perturbational method for estimating frequency response statistics of built-up structures with uncertain properties, Journal of Sound and Vibration V242 (2001) 793–811.
[5] H.A. Jahn, Improvement of an approximate set of latent roots and modal columns of a matrix by methods akin to those of classical perturbation theory, Quarterly Journal of Mechanics and Applied Mathematics 1 (1948) 132–144.
[6] R.L. Fox, M.P. Kapoor, Rates of change of eigenvalues and eigenvectors, American Institute of Aeronautics and Astronautics Journal 6 (1968) 426–2429.
[7] R.M. Lin, M.K. Lim, Derivation of structural design sensitivities from vibration test data, Journal of Sound and Vibration V201 (1997) 613–631.
[8] P. Vanhonacker, Differential and difference sensitivities of natural frequencies and mode shapes of mechanical structures, American Institute of Aeronautics and Astronautics Journal V18 (1980) 1511–1514.

[9] H.V. Belle, Higher order sensitivities in structural systems, American Institute of Aeronautics and Astronautics Journal V20 (1982) 286–288.
[10] A.Q. Liu, S.P. Lim, K.M. Liew, Sensitivity analysis of complex dynamic system modeling, JSME V36 (1993) 209–213.
[11] Z.-Q. Qu, Hybrid expansion method for frequency responses and their sensitivities, Part I: Undamped systems, Journal of Sound and Vibration V231 (2000) 175–193.
[12] Z.-Q. Qu, R.P. Selvam, Hybrid expansion method for frequency responses and their sensitivities, Part II: Viscously damped systems, Journal of Sound and Vibration V238 (2000) 369–388.
[13] C. Yang, D.E. Adams, Embedded sensitivity functions for structural dynamic systems, 21st International Modal Analysis Conference, Kissimmee, FL, 3–6 February 2003.